Research Article | Vol. 26, No. 16 | 6 Aug 2018 | OPTICS EXPRESS 21358
Optics EXPRESS

Picojoule-level octave-spanning supercontinuum generation in chalcogenide waveguides

JEAN-ÉTIENNE TREMBLAY,[1] MARCIN MALINOWSKI,[2] KATHLEEN A. RICHARDSON,[2] SASAN FATHPOUR,[2] AND MING C. WU[1,*]

[1] *Department of Electrical Engineering and Computer Sciences, University of California, Berkeley, CA 94720, USA*
[2] *CREOL, The College of Optics & Photonics, University of Central Florida, Orlando, FL 32816, USA*
[*] *wu@eecs.berkeley.edu*

Abstract: Low propagation loss $Ge_{23}Sb_7S_{70}$ waveguides (0.56 dB/cm) are fabricated in a wafer scale process. Simulation of a 2 cm long, 1.2 µm wide waveguide with 100 ps/nm/km peak dispersion predicts coherent supercontinuum generation at 1.55 µm pump wavelength. Octave-spanning supercontinuum using a dispersive wave is experimentally demonstrated using picojoule-level energy (26 pJ, 240 fs pulse width, 77 W peak power) pulses.

1. Introduction

Supercontinuum generation as a way of generating optical frequency combs has gained significant interest in the past two decades with the invention of the $f-2f$ self-referencing technique [1, 2]. With the recent advances in optical integrated devices, on-chip supercontinuum generation is one of the key elements to enable low power and portable optical synthesizers [3]. Other applications of supercontinuum sources include spectroscopy, telecommunication and optical coherence tomography [2, 4], to name a few.

Octave-spanning supercontinua and frequency combs have now been demonstrated in a broad range of materials and wavelength regions. In the mid-IR region, useful for sensing applications, GeAsSe based waveguides have been used to generate supercontinua spanning several octaves [5]. Chalcogenide glass fibers have also been shown to demonstrate broad IR supercontinuum [6], and recent advances in compositional optimization to tailor bandwidth, dispersion and long term (aging) stability [7, 8] show promise in candidate bulk systems extendable to fibers aimed at reducing the typically high powers needed for fibers due to their large mode sizes.

In the 1 µm–2 µm spectral region, which is of interest because of the readily available and efficient semiconductor sources at 1.55 µm telecommunication wavelength, extensive research on supercontinuum generation has been done on silicon nitride based platforms. Both conventional supercontinuum generation waveguides and optical ring resonators have been demonstrated to generate frequency combs spanning more than one octave [9–11] with pulse energies on the order of less than 100 pJ and 100 fs pulse widths. The very short pulses required to generate the high peak optical powers to achieve octave spanning combs in both cases are still too high for practical, low power and portable optical synthesizer devices. Recently, coherent and low-power octave-spanning supercontinuum has also been demonstrated in silicon [12], requiring pumping at longer wavelength (1.8 µm) to overcome the large two-photon absorption of silicon in the C-band.

Chalcogenide glasses were also used to demonstrated supercontinuum generation in the near-IR. As_2S_3 based waveguides were used to demonstrate low-power supercontinuum generation in the 1 µm–2 µm wavelength range, with a −30 dB bandwidth close to one octave [13]. Some concerns about As-based materials are their toxicity and the photo-darkening effect [14] they exhibit. In this work we fabricate devices using $Ge_{23}Sb_7S_{70}$, which does not oxidize in air and does not show

#336171 https://doi.org/10.1364/OE.26.021358
Journal © 2018 Received 11 Jul 2018; accepted 17 Jul 2018; published 3 Aug 2018

Optics EXPRESS

any photodarkening effect unlike other chalcogenides [15]. Octave spanning supercontinuum generation has already been demonstrated in this material [16].

We report on the fabrication of low-loss $Ge_{23}Sb_7S_{70}$ waveguides. By careful engineering of waveguide dispersion, we demonstrate octave-spanning supercontinuum pumped at 1.55 µm with picojoule-level pulse energy. Simulations show that the measured spectrum is coherent at f and $2f$ wavelengths.

2. Fabrication and material properties

2.1. Fabrication process

The chalcogenide waveguides are fabricated with a 6" wafer-scale process with DUV lithography at the UC Berkeley Marvell Nanofabrication Laboratory. We start with a silicon wafer with 2.5 µm of thermal oxide as the bottom cladding layer. A silicon nitride spot-size converter layer [17] is then fabricated using either plasma-enhanced chemical vapor deposition (PECVD) silicon nitride and etching, or by the photonic damascene process [18].

The GeSbS bulk material is fabricated using melt quench technique [19]. It is then thermally evaporated at a rate of 50 nm/min, and the composition of the film was verified by energy-dispersive X-ray spectroscopy to differ from the bulk material by less than 1 %. Several dry etching chemistries, such as chlorine- and fluorine-based plasmas [20], can etch effectively GeSbS. In this work, we use a mixture of CHF_3 and O_2 in a reactive ion etcher (RIE) to get smooth and vertical waveguide sidewalls.

A final PECVD SiO_2 cladding layer is deposited on top of the chalcogenide waveguides at 250 °C. The devices are cut using stealth dicing technology, with the coupling waveguide stitched across the dies. Figure 1 shows a cross section of the diced facet, with near vertical sidewalls for the chalcogenide waveguide. After dicing, we apply an anti-reflective coating to the facet by depositing 100 nm of PECVD SiO_2 on the chips.

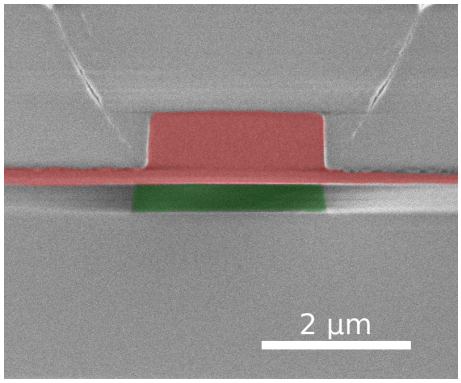

Fig. 1. SEM cross section of the fabricated devices. Red: $Ge_{23}Sb_7S_{70}$ rib waveguide. Green: Si_3N_4 spot size converter layer.

2.2. Propagation loss and dispersion

We include ring resonator structures in the chalcogenide layer in order to measure the propagation loss and dispersion of the GeSbS waveguides. The finesse of the resonances is used to determine the propagation loss, and the group index (and thus the dispersion) is calculated from the free spectral range. The measured ring resonator has a waveguide width of 1.8 µm and a ring radius of 100 µm. An optical vector analyzer (Luna OVA 5000) is used to scan the C and L band insertion loss over both TE and TM polarizations.

Optics EXPRESS

Figure 2 shows the dispersion calculated from the ring free spectral ranges for both fundamental TE and TM modes. The simulated dispersion using a finite difference mode solver for a waveguide with the same dimensions (1.8 µm wide rib waveguide) is shown as a reference, with good agreement over the C and L band for both TE and TM modes, indicating that the material dispersion model is accurate.

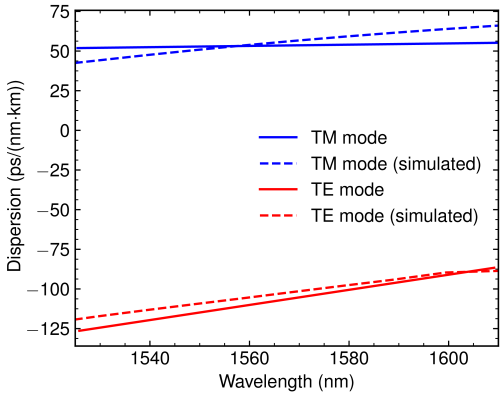

Fig. 2. Comparison of simulated dispersion with dispersion measured using the ring resonator FSR method, showing agreement for both TE and TM modes.

Figure 3(a) shows an example of a ring resonance with a FWHM of (2.07 ± 0.01) pm, corresponding to a unloaded quality factor of $(1.018 \pm 0.007) \times 10^6$. The extracted propagation loss is (0.398 ± 0.003) dB/cm, similar to previously reported values in the same material [20–22]. The linear propagation loss of waveguides can also be measured using an OFDR technique [23]. The slope of the backscattered light with respect to distance represents twice the linear attenuation of the waveguide. We used a commercial tool (OVA 5000) to measure 4 cm long, 1.2 µm wide rib waveguides. The measured reflected light is shown on Figure 3(b). The two major peaks represent the facet reflections. The backscattered signal decreases with a constant slope, meaning that the bending loss is negligible. The extracted propagation loss is (0.56 ± 0.05) dB/cm, which is slightly higher than the measured loss from the ring resonator with 1.8 µm wide waveguide.

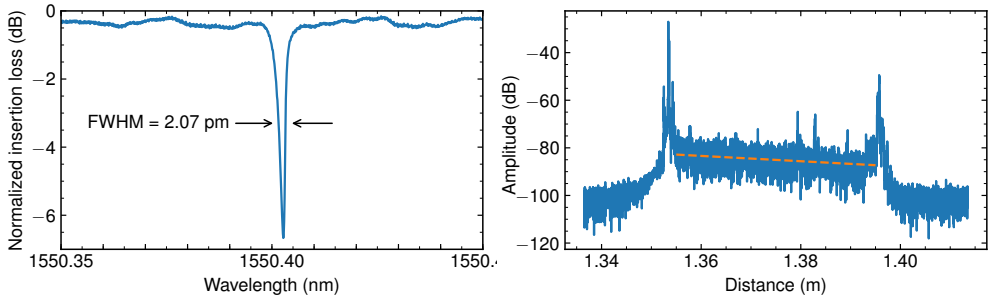

Fig. 3. Waveguide propagation loss measured using (a) ring resonator quality factor and (b) OFDR backscattering signal. The quality factor is over 10^6 and the extracted propagation loss is 0.56 dB/cm.

Optics EXPRESS

3. Results

3.1. Supercontinuum generation simulation

Efficient supercontinuum generation usually happens when the waveguide operates in the anomalous dispersion regime [24]. We engineered a chalcogenide rib waveguide with a SiO_2 cladding that has a fundamental quasi-TM mode with anomalous dispersion of 100 ps/nm/km at 1.65 µm wavelength. The rib width is 1.2 µm, the rib height is 910 nm, and the slab height is 240 nm. The simulated dispersion for this waveguide is shown in Figure 4. The blue side and red side zero dispersion wavelengths from the 1.55 µm pump wavelength are respectively 1.35 µm and 2.10 µm. Based on the phase-matching condition at low soliton numbers [25], the dispersive waves are expected to appear near 1.1 µm and 2.9 µm.

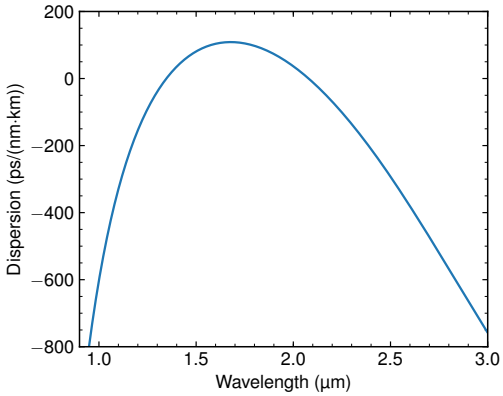

Fig. 4. Simulated dispersion for 1.2 µm wide waveguide, showing 100 ps/nm/km dispersion peak around 1.65 µm, and zero-dispersion wavelengths of 1.35 µm and 2.10 µm

The supercontinuum generation in the GeSbS waveguide is simulated using the standard split-step Fourier method. The nonlinear parameters are taken from [15, 22]. Higher-order dispersion, self-steepening and Raman effects are taken into account. The simulated spectrum is shown on Figure 5(a), using 26 pJ pulses, 240 fs pulse width and 2 cm propagation length. The coherence properties of the supercontinuum are studied by comparing an ensemble of simulated output pulses with quantum limited noise on the input pulse [26]. The resulting $|g_{12}|$ coherence is shown on Figure 5(b), and is near-unity from 1 µm to 3 µm.

3.2. Experimental spectrum

A commercial femtosecond erbium-doped fiber laser (Calmar) is used to pump the fabricated waveguides at 1.55 µm wavelength. The laser repetition rate is 25 MHz and the minimum pulse width is 240 fs after amplification and linear compression. The light is coupled in and out the device using lensed fibers, and the generated spectrum is measured using a spectrometer (Ocean Optics NIRQuest, 0.9 µm-2.5 µm). The output spectrum for 3.2 mW average amplified laser power is shown on Figure 5(a), superimposed on the simulation. The spectrometer noise floor is −40 dBm, and the 2.5 µm long wavelength limit does not permit to see the 2.9 µm dispersive wave predicted by simulation. The measured supercontinuum extends from 1.03 µm to at least 2.08 µm (noise floor limited), which is greater than one octave required for $f-2f$ self-referencing, and shows very good agreement with the simulation on the dispersive wave amplitude and wavelength. The minor discrepancies between both spectra can be explained by the assumptions about the Raman gain properties of the material, which were not directly measured. More importantly,

Optics EXPRESS

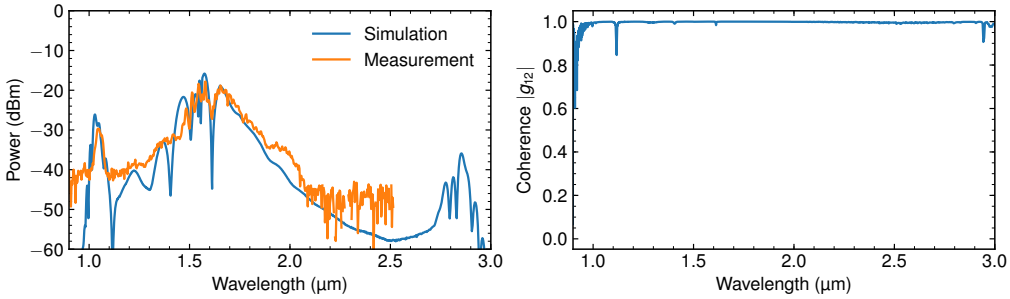

(a) (b)

Fig. 5. Low pulse energy supercontinuum generation and simulation. (a) Simulation of 26 pJ pulses after 2 cm propagation, overlapped on the experimental spectrum. The spectrometer bandwidth is limited to 0.9 μm to 2.5 μm. (b) Coherence properties of the simulated supercontinuum, showing near-unity coherence both at the 1.03 μm dispersive wave end and the 2.06 μm end of the supercontinuum.

considering a typical waveguide coupling loss of (7 ± 1) dB, the experimental waveguide pulse energy is between 20 pJ and 32 pJ, which is commensurate with the 26 pJ pulse energy used in the simulation. Compared to [15], this work demonstrates an octave-spanning supercontinuum with much lower pulse energy by optimizing the waveguide geometry to generate a dispersive wave at the short wavelength end. Moreover, due to the low pulse energy, the generated supercontinuum shows near-unity coherence in simulation.

4. Conclusion

We designed and fabricated $Ge_{23}Sb_7S_{70}$ rib waveguides for supercontinuum generation. Dispersion is measured using ring resonators and shows good agreement with simulation. The chalcogenide waveguides have a low loss of 0.56 dB/cm measured using OFDR technique. Coherent, octave-spanning supercontinuum is simulated with pulse energies as low as 26 pJ with 240 fs pulse length. The octave-spanning supercontinuum is measured experimentally, spanning from 1.03 μm to at least 2.08 μm. The high nonlinearity of chalcogenide glasses is important in reducing the required pulse energy and peak power as well as relaxing the pulse length required for coherent supercontinuum generation compared to other near-IR low-loss materials such as silicon nitride. Moreover, the large transparency window of chalcogenide glasses compared to silicon permits the use of convenient telecom wavelength femtosecond laser sources, which is critical in developing low power integrated frequency comb sources.

Funding

Defense Advanced Research Project Agency (DARPA) (HR0011-15-C-0057).

References

1. D. J. Jones, S. A. Diddams, J. K. Ranka, A. Stentz, R. S. Windeler, J. L. Hall, and S. T. Cundiff, "Carrier-envelope phase control of femtosecond mode-locked lasers and direct optical frequency synthesis," Science **288**, 635–639 (2000).
2. T. Udem, R. Holzwarth, and T. W. Hansch, "Optical frequency metrology," Nature **416**, 233–237 (2002).
3. D. T. Spencer, T. Drake, T. C. Briles, J. Stone, L. C. Sinclair, C. Fredrick, Q. Li, D. Westly, B. R. Ilic, A. Bluestone, N. Volet, T. Komljenovic, L. Chang, S. H. Lee, D. Y. Oh, M.-G. Suh, K. Y. Yang, M. H. P. Pfeiffer, T. J. Kippenberg, E. Norberg, L. Theogarajan, K. Vahala, N. R. Newbury, K. Srinivasan, J. E. Bowers, S. A. Diddams, and S. B. Papp, "An optical-frequency synthesizer using integrated photonics," Nature **557**, 81–85 (2018).

Optics EXPRESS

4. A. F. Fercher, W. Drexler, C. K. Hitzenberger, and T. Lasser, "Optical coherence tomography - principles and applications," Reports on Prog. Phys. **66**, 239 (2003).
5. Y. Yu, X. Gai, P. Ma, D.-Y. Choi, Z. Yang, R. Wang, S. Debbarma, S. J. Madden, and B. Luther-Davies, "A broadband, quasi-continuous, mid-infrared supercontinuum generated in a chalcogenide glass waveguide," Laser & Photonics Rev. **8**, 792–798 (2014).
6. S. Shabahang, A. Sims, G. Tao, L. Shah, M. Richardson, and A. Abouraddy, "Multi-octave mid-infrared supercontinuum generation in robust chalcogenide nanowires using a thulium fiber laser," in *Photonics and Fiber Technology 2016 (ACOFT, BGPP, NP),* (Optical Society of America, 2016), p. AT2C.2.
7. O. Mouawad, P. Béjot, F. Billard, P. Mathey, B. Kibler, F. Désévédavy, G. Gadret, J.-C. Jules, O. Faucher, and F. Smektala, "Mid-infrared filamentation-induced supercontinuum in As–S and an As-free Ge–S counterpart chalcogenide glasses," Appl. Phys. B **121**, 433–438 (2015).
8. O. Mouawad, P. Béjot, F. Billard, P. Mathey, B. Kibler, F. Désévédavy, G. Gadret, J.-C. Jules, O. Faucher, and F. Smektala, "Filament-induced visible-to-mid-IR supercontinuum in a ZnSe crystal: Towards multi-octave supercontinuum absorption spectroscopy," Opt. Mater. **60**, 355–358 (2016).
9. A. R. Johnson, A. S. Mayer, A. Klenner, K. Luke, E. S. Lamb, M. R. E. Lamont, C. Joshi, Y. Okawachi, F. W. Wise, M. Lipson, U. Keller, and A. L. Gaeta, "Octave-spanning coherent supercontinuum generation in a silicon nitride waveguide," Opt. Lett. **40**, 5117–5120 (2015).
10. Q. Li, T. C. Briles, D. Westly, J. Stone, R. Ilic, S. Diddams, S. Papp, and K. Srinivasan, "Octave-spanning microcavity Kerr frequency combs with harmonic dispersive-wave emission on a silicon chip," in *Frontiers in Optics 2015,* (Optical Society of America, 2015), p. FW6C.5.
11. D. R. Carlson, D. D. Hickstein, A. Lind, S. Droste, D. Westly, N. Nader, I. Coddington, N. R. Newbury, K. Srinivasan, S. A. Diddams, and S. B. Papp, "Self-referenced frequency combs using high-efficiency silicon-nitride waveguides," Opt. Lett. **42**, 2314–2317 (2017).
12. N. Singh, M. Xin, D. Vermeulen, K. Shtyrkova, N. Li, P. T. Callahan, E. S. Magden, A. Ruocco, N. Fahrenkopf, C. Baiocco, B. P.-P. Kuo, S. Radic, E. Ippen, F. X. Kärtner, and M. R. Watts, "Octave-spanning coherent supercontinuum generation in silicon on insulator from 1.06 μm to beyond 2.4 μm," Light. Sci. &Amp; Appl. **7**, 17131 (2018).
13. M. R. Lamont, B. Luther-Davies, D.-Y. Choi, S. Madden, and B. J. Eggleton, "Supercontinuum generation in dispersion engineered highly nonlinear (γ = 10 /w/m) As2S3 chalcogenide planar waveguide," Opt. Express **16**, 14938–14944 (2008).
14. G. Pfeiffer, M. Paesler, and S. Agarwal, "Reversible photodarkening of amorphous arsenic chalcogens," J. Non-Crystalline Solids **130**, 111–143 (1991).
15. J. W. Choi, Z. Han, B.-U. Sohn, G. F. R. Chen, C. Smith, L. C. Kimerling, K. A. Richardson, A. M. Agarwal, and D. T. H. Tan, "Nonlinear characterization of GeSbS chalcogenide glass waveguides," Sci. Reports **6**, 39234 (2016).
16. M. Malinowski, J. E. Tremblay, G. F. C. Gonzalez, A. Rao, S. Khan, P. K. Hsu, A. Yadav, K. A. Richardson, P. Delfyett, M. C. Wu, and S. Fathpour, "Amplified octave-spanning supercontinuum from chalcogenide waveguides for second-harmonic generation," in *2017 IEEE Photonics Conference (IPC),* (2017).
17. J. E. Tremblay, Y. H. Lin, P. K. Hsu, M. Malinowski, S. Novak, P. Qiao, G. F. Camacho-Gonzalez, C. Chang-Hasnain, K. Richardson, S. Fathpour, and M. C. Wu, "Large bandwidth silicon nitride spot-size converter for efficient supercontinuum coupling to chalcogenide waveguide," in *2017 Conference on Lasers and Electro-Optics (CLEO),* (2017).
18. M. H. P. Pfeiffer, A. Kordts, V. Brasch, M. Zervas, M. Geiselmann, J. D. Jost, and T. J. Kippenberg, "Photonic damascene process for integrated high-q microresonator based nonlinear photonics," Optica **3**, 20–25 (2016).
19. L. Petit, N. Carlie, F. Adamietz, M. Couzi, V. Rodriguez, and K. Richardson, "Correlation between physical, optical and structural properties of sulfide glasses in the system Ge-Sb-S," Mater. Chem. Phys. **97**, 64–70 (2006).
20. J. Chiles, M. Malinowski, A. Rao, S. Novak, K. Richardson, and S. Fathpour, "Low-loss, submicron chalcogenide integrated photonics with chlorine plasma etching," Appl. Phys. Lett. **106**, 111110 (2015).
21. Q. Du, Y. Huang, J. Li, D. Kita, J. Michon, H. Lin, L. Li, S. Novak, K. Richardson, W. Zhang, and J. Hu, "Low-loss photonic device in Ge–Sb–S chalcogenide glass," Opt. Lett. **41**, 3090–3093 (2016).
22. S. Serna, H. Lin, C. Alonso-Ramos, A. Yadav, X. Le Roux, K. Richardson, E. Cassan, N. Dubreuil, J. Hu, and L. Vivien, "Nonlinear optical properties of integrated GeSbS chalcogenide waveguides," Photonics Res. **6**, B37 (2018).
23. B. J. Soller, D. K. Gifford, M. S. Wolfe, and M. E. Froggatt, "High resolution optical frequency domain reflectometry for characterization of components and assemblies," Opt. Express **13**, 666–674 (2005).
24. G. P. Agrawal, *Nonlinear Fiber Optics* (Academic Press, 2012), 5th ed.
25. D. R. Austin, C. M. de Sterke, B. J. Eggleton, and T. G. Brown, "Dispersive wave blue-shift in supercontinuum generation," Opt. Express **14**, 11997–12007 (2006).
26. J. M. Dudley and S. Coen, "Coherence properties of supercontinuum spectra generated in photonic crystal and tapered optical fibers," Opt. Lett. **27**, 1180–1182 (2002).